Gram-scale Solvothermal Synthesis of Fe-doped $CuCoO_2$ Nanosheets and Improvement of Oxygen Evolution Reaction Performance

Miao Yang,[a] Hao Tan,[a,b] Shiyu Ma,[a] Yue Mi,[a] Lifeng Liu,[b] Zongyan Zhao,[c] Hong Li[a] and Dehua Xiong,[a]*

a. State Key Laboratory of Silicate Materials for Architectures, Wuhan University of Technology, Wuhan 430070, P. R. China.

b. Songshan Lake Materials Laboratory, Dongguan, 523808, P. R. China.

c. Faculty of Materials Science and Engineering, Kunming University of Science and Technology, Kunming 650093, P. R. China.

* Corresponding author email: xiongdehua2010@gmail.com

Experimental Details

Materials synthesis

All chemicals in the experiment were of analytical grade without further purification. Cu-BTC-IPA and $CuCoO_2$ were prepared according to our previous work[1].

Cu-BTC-IPA synthesis: Firstly, 2.6093 g $Cu(NO_3)_2 \cdot 3H_2O$, 1.26 g H_3BTC and 9 mL isopropyl alcohol (IPA) were dissolved in 27 mL deionized solution (DI) and 36mL absolute ethanol (ET), and magnetically stirring for 30 minutes. Secondly, the solution was transferred into a Teflon lined autoclave and kept at 120 °C for 12 h. Afterward, the obtained blue precipitate was washed three times with ET to remove any by-product impurities. Finally, the as-prepared Cu-BTC-IPA was dried at 70 °C for 5 h for further using.

Delafossite $CuCoO_2$ synthesis: Cu-BTC-IPA $Co(NO_3)_2 \cdot 6H_2O$ and NaOH were dissolved in 20 mL DI and 50 mL ET, and magnetically stirred for 30 minutes. Then 30 mmol PVP (or not) was added to the above solution and stirred for 1h, and then transferred the solution to a Teflon lined autoclave as well as kept at 140 °C for 24 h. The obtained precipitate was washed several times with ammonia, DI, and ET, and then dried at 70 °C for 5 h.

Fe-doped $CuCoO_2$ synthesis: Fe-doped $CuCoO_2$ was synthesized based on the preparation of pure $CuCoO_2$. Typically, 1.50 g Cu-BTC-IPA, 5.5 mmol (1.60 g) $Co(NO_3)_2 \cdot 6H_2O$ and 5.5x mmol $FeCl_2 \cdot 4H_2O$ (the values of x are 0.01, 0.03, and 0.05) were dissolved sequentially in 20 mL DI and 50 mL ET at room temperature, 1.40 g NaOH and 30 mmol PVP (K23-27) were added to the above solution, and the reaction took place at 140 °C for 24 hours. Finally, the as-obtained $CuCoO_2$-based samples were washed several times with deionized water and ethanol, and then dried at 70 °C for 5 h.

Structural characterization

The crystal phase of samples was characterized by the powder X-ray diffraction (XRD, D8 Advance). The morphology, microstructure, and chemical composition of the samples were examined by field-emission scanning electron microscopy (FESEM,

S4800, produced by Hitachi, Japan) and transmission electron microscopy (TEM, JEOL JEM-2100 operating at 200 keV) equipped with energy-dispersive X-ray spectroscopy (EDX). The surface chemical states of $CuCoO_2$-based powders and Ni@3FCCO working electrodes were analyzed by X-ray photoelectron spectroscopy (XPS, Thermo Escalab 250Xi). The Al Kαradiator (Ephoton = 1486.6 eV) was used in the XPS test. The filament current was 10 m A and the filament voltage energy was 14.7 keV. The C 1s line (284.80 eV) corresponding to the surface adventitious carbon (C-C line bond) has been used as the reference binding energy. The structure of samples was investigated by Raman (LABHRev-UV). The Brunauer-Emmett-Teller (BET) specific surface areas and porosity parameters of the samples were taken by N_2 adsorption-desorption isothermetry (Micromeritics TriStar II 3020 3.02). The element proportion of the samples was analyzed by inductively coupled plasma-atomic emission spectrometry (ICP-AES, Prodigy 7). An atomic force microscopy (AFM) with DI Nanoscope IV controller (Veeco, USA) was used to record the AFM height images of the sample.

Electrode preparation and electrochemical measurement

The OER performance was evaluated by cyclic voltammetry (CV) and electrochemical impedance spectroscopy (EIS) in a three-electrode configuration in 1.0 M KOH (pH = 13.5) using a CS2350H electrochemical workstation (Wuhan Corrtest Instruments Corp., China). A platinum wire and a saturated calomel electrode (SCE) were used as the counter and reference electrodes, respectively. To prepare the nickel (Ni) foam supported CCO and xFCCO based NSs (Ni@CCO and Ni@xFCCO, x=1, 3, and 5.) working electrodes, 15 mg Fe-doped or pure $CuCoO_2$ powders were dispersed in a mixture of 500 μL water, 480 μL isopropanol and 20 μL Nafion (5 wt%, Sigma). An appropriate amount of suspension was then drop cast on to the surface of the Ni foam sheets (surface area: 1.0 cm^2), and the working electrode was dried at 150 °C for 10 minutes. Cyclic voltammetric (CV) scans were recorded between 1.05 and 1.80 V vs. reversible hydrogen electrode (RHE) at a scan rate of 2 $mV \cdot s^{-1}$. The electrochemical double-layer capacitance (C_{dl}) can be extracted through CV scans recorded at different

rates (from 20 to 100 $mV \cdot s^{-1}$) in the non-faradaic potential window of -0.05-0.05 V vs. SCE. The EIS measurements were performed in the frequency range of 100 kHz-10 mHz under a constant potential of 1.63 V vs. RHE.

All current density values are normalized with respect to the geometrical surface area of the working electrode. All CV curves presented in this work are *iR*-corrected (85%). The correction was done according to the following equation:

$$E_c = E_m - iR_s \quad \text{(S1)}$$

where E_c is the *iR*-corrected potential, E_m experimentally measured potential, and R_s the equivalent series resistance extracted from the electrochemical impedance spectroscopy measurements. Unless otherwise specified, all potentials are reported versus reversible hydrogen electrode (RHE) by converting the potentials measured vs. SCE according to the following formula:

$$E\,(\text{RHE}) = E\,(\text{SCE}) + 0.241 + 0.059\,\text{pH} \quad \text{(S2)}$$

Theoretical calculation details

The spin-polarized DFT calculations were performed by using the Vienna ab initio Simulation Package (VASP). The Kohn–Sham wave functions were expanded in a plane wave basis set with a cutoff energy of 550 eV. The projector-augmented wave (PAW) method and PBE potential for the exchange-correlation functional were used. The Brillouin zone was sampled by the 3 × 3 × 1 Monkhorst-Pack k-point mesh. All atoms were allowed to relax until the forces fell below 0.01 eV Å-1. A vacuum region of 15 Å was created to ensure negligible interaction between mirror images. The ZPE and entropy corrections were included by calculating the phonons by the using the Phonopy.

In an alkaline environment, the widely accepted method to model the OER process is based on a four-electron reaction pathway, which can be summarized as follows: i) formation of *OH on the catalyst surface, ii) formation of *O by deprotonation of *OH, iii) *O oxidation to *OOH, and iv) O_2 formation and release. Here, *OH, *O, and *OOH represent different adsorbed intermediates. For each step, the Gibbs free energy ΔGi (i = 1, 2, 3, 4) can be calculated using equation (3):

$$\Delta G_i = \Delta E + \Delta E_{ZPE} - T\Delta S - e\phi + K_B T \ln(H^+) \quad \text{(S3)}$$

where ΔE is the total energy difference between the reactant and product molecules. ΔE_{ZPE} and $T\Delta S$ are the changes in the zero-point energy and the entropic contribution, respectively. e represents the charge transfer, ϕ is the external potential, and K_B refers to the Boltzmann constant. The $K_B T ln(H^+)$ is the corrected Gibbs free energy of H ions. All reaction free energies were obtained under standard conditions (ϕ = 0, T = 298.15 K, pH = 13.5) using DFT calculations.

The thermodynamic overpotential η is an important electrocatalytic parameter. Low values of η would yield better OER performance electrocatalysts. Based on the above free energy results, the overpotential η for a given electrocatalyst can be determined according to equation (4):

$$\eta = \max[\Delta G_1, \Delta G_2, \Delta G_3, \Delta G_4]/e - 1.23 \text{ V} \quad \text{(S4)}$$

Supplementary tables:

Table S1. Detailed reaction conditions were employed to synthesize Cu-BTC-IPA derived $CuCoO_2$ nanocrystals.

<table>
<tr><th>No.</th><th>Cu-BTC-IPA (g)</th><th>$Co(NO_3)_2$ (g)</th><th>NaOH (g)</th><th>PVP (30 mmol)</th><th>$FeCl_2$ (mmol)</th><th>Solvent (mL)</th><th>Temp. (°C)</th><th>Time (h)</th></tr>
<tr><td>1#</td><td>0.20</td><td>0.16</td><td rowspan="9">5.40</td><td rowspan="15">-</td><td rowspan="22">-</td><td rowspan="22">50 ET:20 DI</td><td rowspan="22">140</td><td rowspan="22">24</td></tr>
<tr><td>2#</td><td>0.40</td><td>0.32</td></tr>
<tr><td>3#</td><td>2.00</td><td rowspan="8">1.60</td></tr>
<tr><td>4#</td><td>1.90</td></tr>
<tr><td>5#</td><td>1.80</td></tr>
<tr><td>6#</td><td>1.70</td></tr>
<tr><td>7#</td><td>1.60</td></tr>
<tr><td>8#</td><td>1.50</td></tr>
<tr><td>9#</td><td>1.40</td></tr>
<tr><td>10#</td><td rowspan="13">1.50</td><td rowspan="13">1.60</td><td>7.40</td></tr>
<tr><td>11#</td><td>6.40</td></tr>
<tr><td>12#</td><td>4.40</td></tr>
<tr><td>13#</td><td>3.40</td></tr>
<tr><td>14#</td><td>2.40</td></tr>
<tr><td>15#</td><td rowspan="6">1.40</td></tr>
<tr><td>16#</td><td>K16-18</td></tr>
<tr><td>17#</td><td>K23-27</td></tr>
<tr><td>18#</td><td>K30</td></tr>
<tr><td>19#</td><td rowspan="3">K23-27</td><td>0.055</td></tr>
<tr><td>20#</td><td>0.165</td></tr>
<tr><td>21#</td><td>0.275</td></tr>
</table>

Table S2. The OER performance of CCO based electrodes in this paper in comparison to other oxide catalysts.

Catalyst	Electrolyte	η_{10} (mV)	Tafel slope (mV dec^{-1})	(year)[Ref.]
Bare Ni	1.0 M KOH	538	142	This work
Ni@CCO		454	95	
Ni@1FCCO		413	90	
Ni@3FCCO		369	69	
Ni@5FCCO		393	87	
glassy carbon@CCO		440	92.8	(2018)[2]
glassy carbon@CCO-PVP		390	70	(2019)[3]
Ni@CCaCO-PVP		470	96.5	(2020)[4]
Ni@CCO(IPA)		467	101	(2023)[1]
Ni@5NCCO		409	98	(2022)[5]
Ni@$CuScO_2$		470	114	(2020)[6]
glassy carbon@$AgCoO_2$		395	-	(2019)[7]
glassy carbon@$CuFeO_2$		-	49.4	(2022)[8]
glassy carbon@$La_{1-x}Sr_xCoO_{3-\delta}$		326	70.8	(2018)[9]
glassy carbon@$La_{0.9}Sn_{0.1}NiO_{3-\delta}$		318	74	(2022)[10]
glassy carbon@$La_{0.9}Ce_{0.1}NiO_3$		270	45	(2021)[11]
glassy carbon@ $Sr_2Fe_{1.5-x-y}Co_xNi_yMo_{0.5}O_{6-\delta}$	0.1 M KOH	400	84	(2019)[12]
glassy carbon@$LaNiO_3$		550	148	(2019)[13]
glassy carbon@$LaNi_{0.85}Mg_{0.15}O_3$		450	95	(2019)[13]
glassy carbon@$LaCoO_3$		680 vs Ag/AgCl	74.4	(2019)[14]
glassy carbon@$LaCo_{0.9}Ni_{0.1}O_3$		650 vs Ag/AgCl	62.2	(2019)[14]

Supplementary figures:

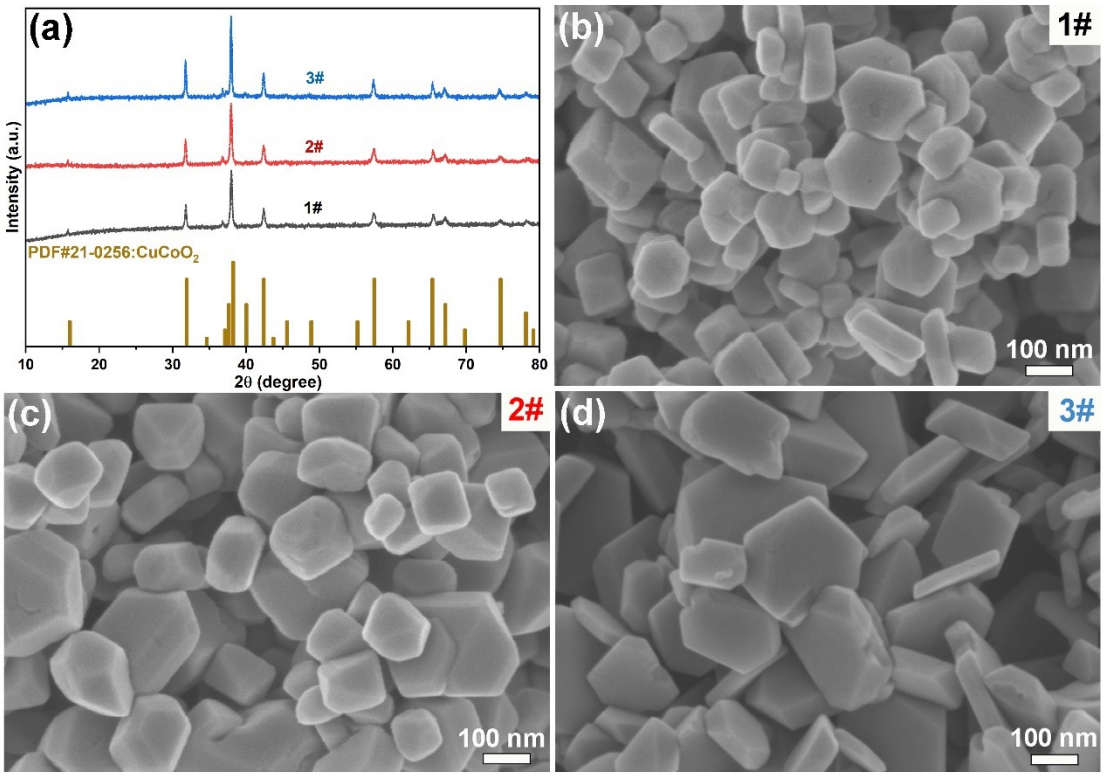

Fig. S1. XRD patterns (a) and SEM images (b-c) of Cu-BTC-IPA derived $CuCoO_2$ crystals synthesized at different reactants concentrations (1#, ×1; 2#, ×2; 3#, ×10).

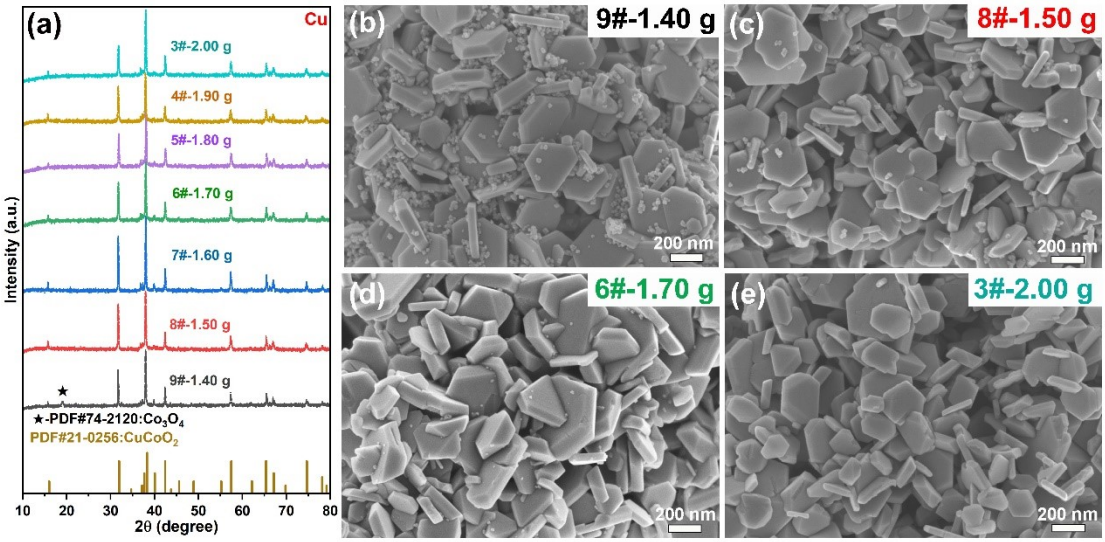

Fig. S2. The XRD patterns (a) and SEM images (b, 1.40g; c, 1.50g; d, 1.70g; e, 2.00g) of Cu-BTC-IPA derived $CuCoO_2$ crystals with different amounts of copper source (1.40 ~ 2.00 g).

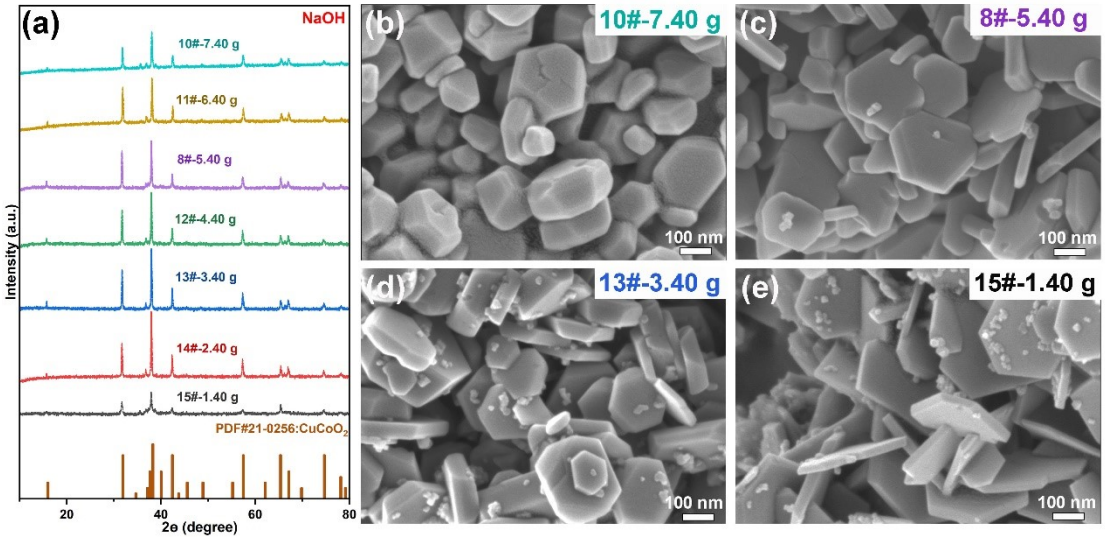

Fig. S3. XRD patterns (a) and SEM images (b-e) of Cu-BTC-IPA derived $CuCoO_2$ crystals with different amount of NaOH additions (1.40 ~ 7.40 g).

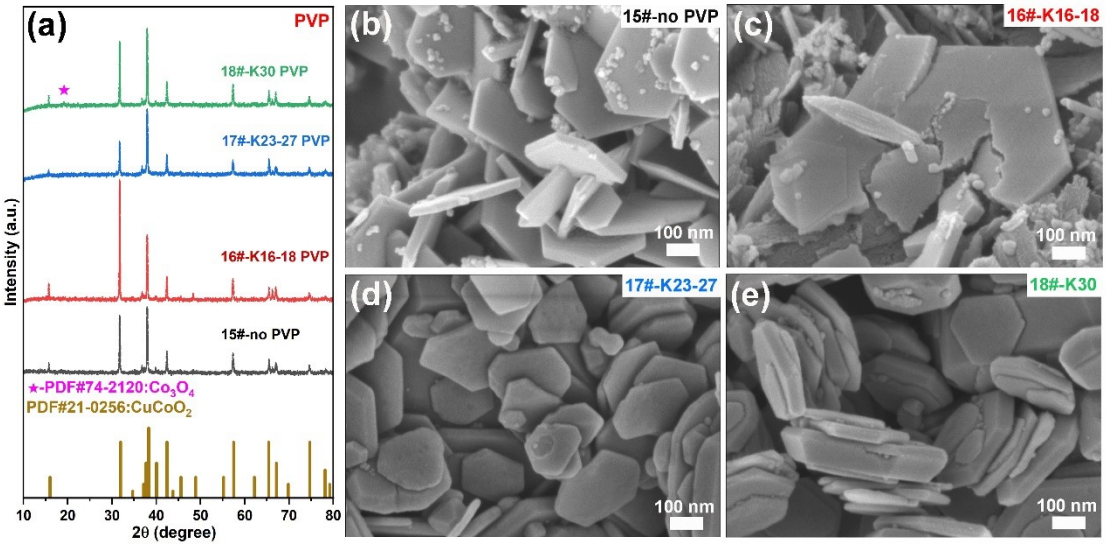

Fig. S4. XRD patterns (a) and SEM images (b-e) of Cu-BTC-IPA derived $CuCoO_2$ crystals with different K values of PVP surfactants.

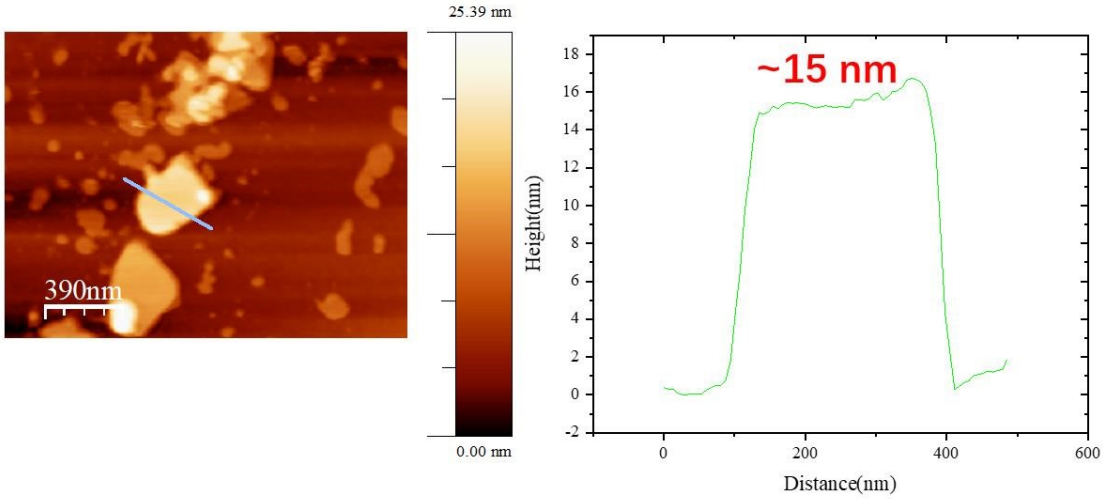

Fig. S5. AFM image and curve diagram showing thickness distribution of 3FCCO.

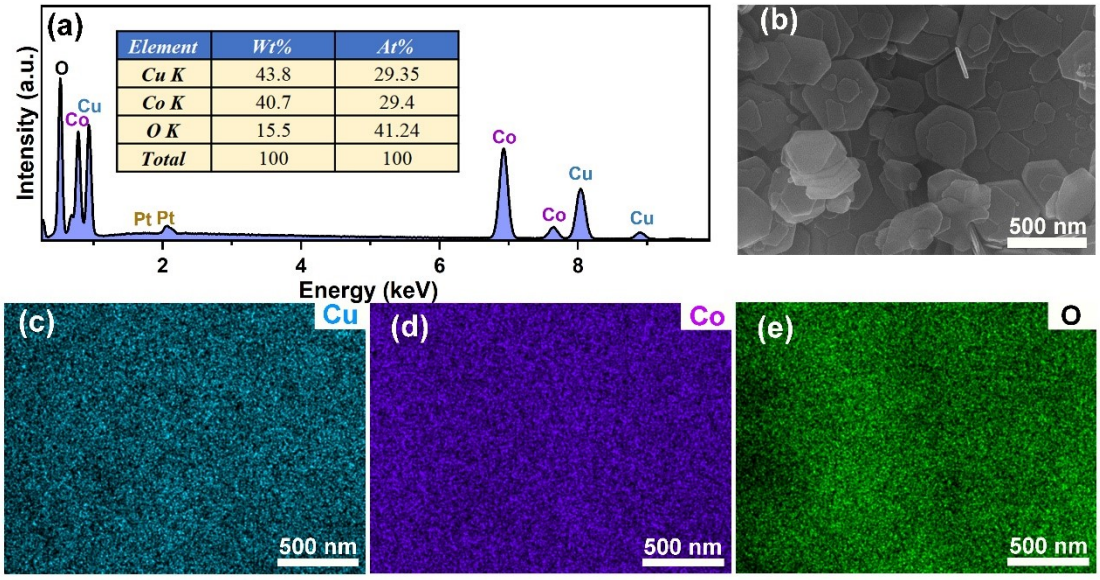

Fig. S6. EDX spectrum (a), SEM images (b) and elemental maps (c-e) of CCO powder.

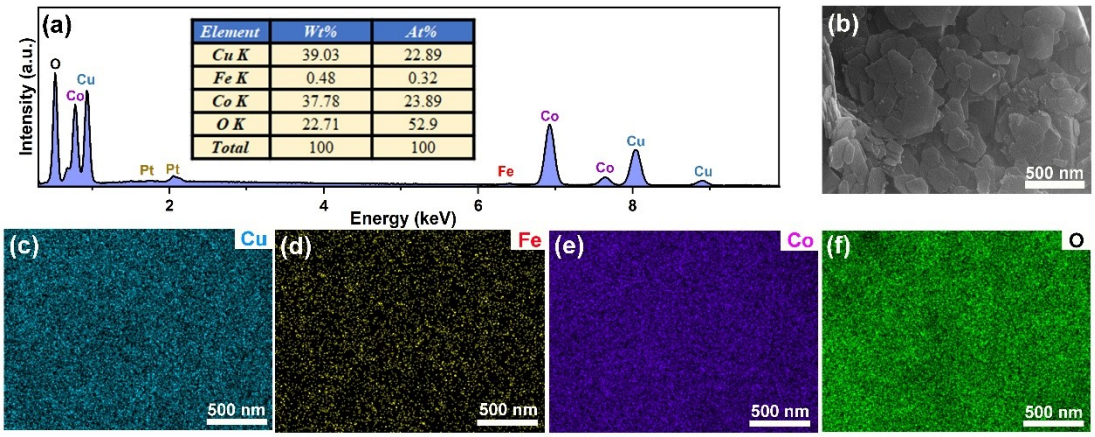

Fig. S7. EDX spectrum (a), SEM images (b) and elemental maps (c-f) of 1FCCO powder.

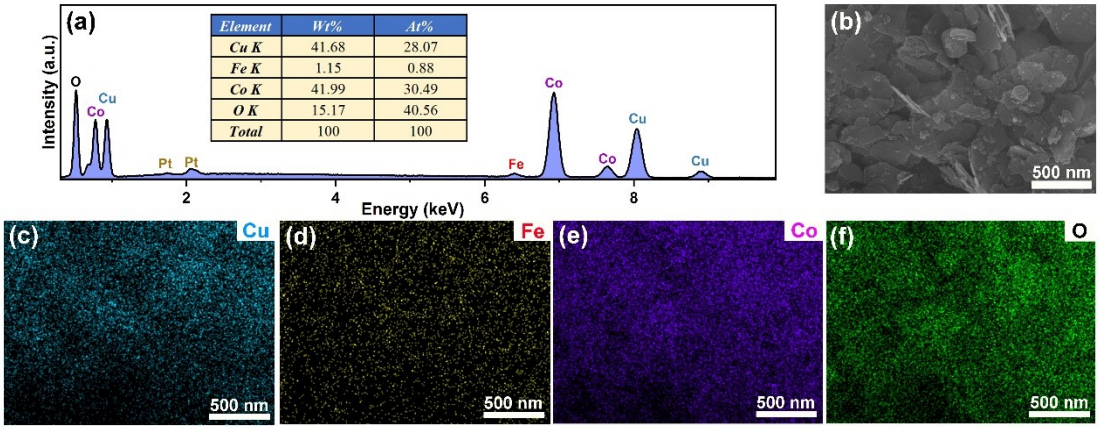

Fig. S8. EDX spectrum (a), SEM images (b) and elemental maps (c-f) of 3FCCO powder.

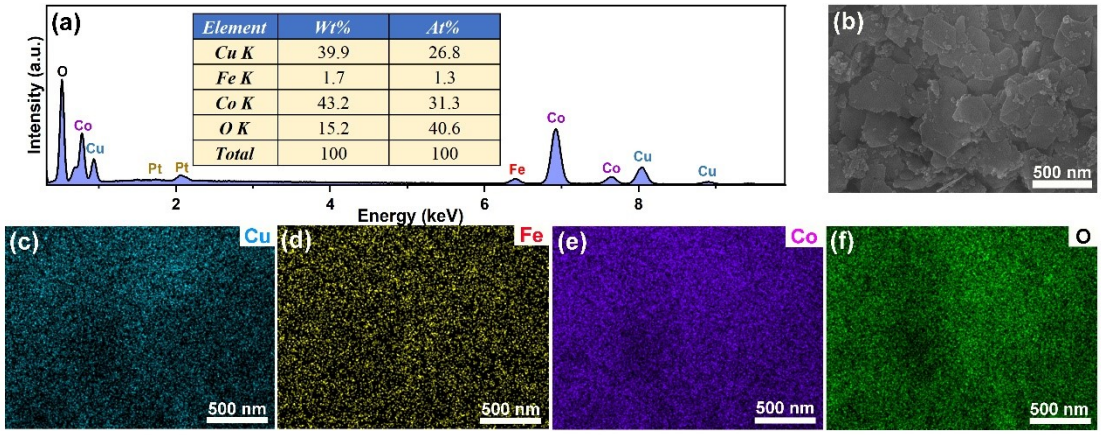

Fig. S9. EDX spectrum (a), SEM images (b) and elemental maps (c-f) of 5FCCO powder.

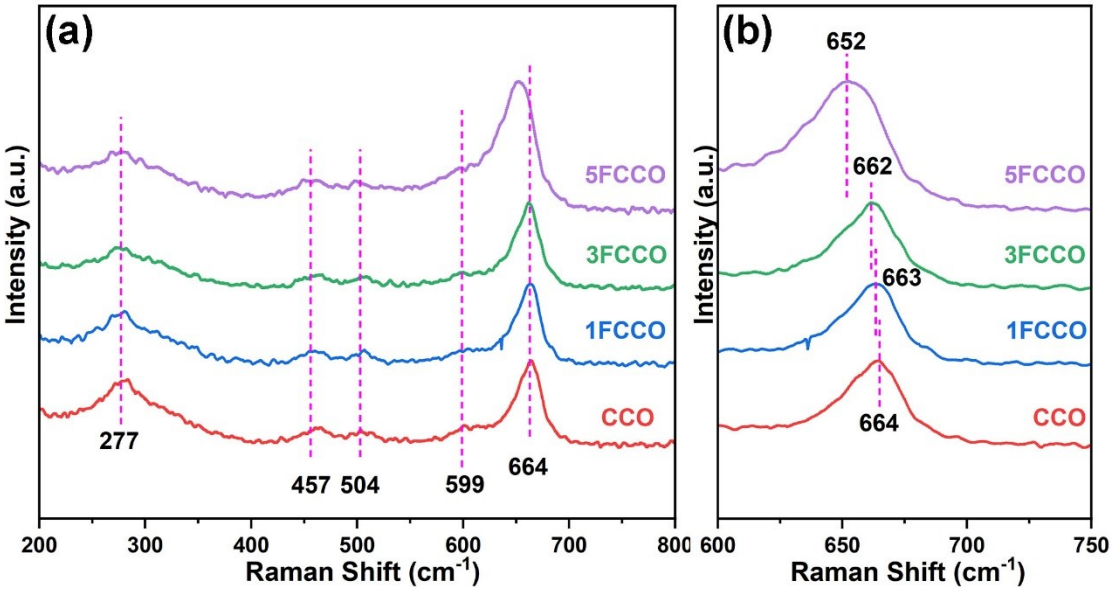

Fig. S10. Raman spectrum (a) and the partially enlarged drawing (b) of CCO, 1FCCO, 3FCCO and 5FCCO powders.

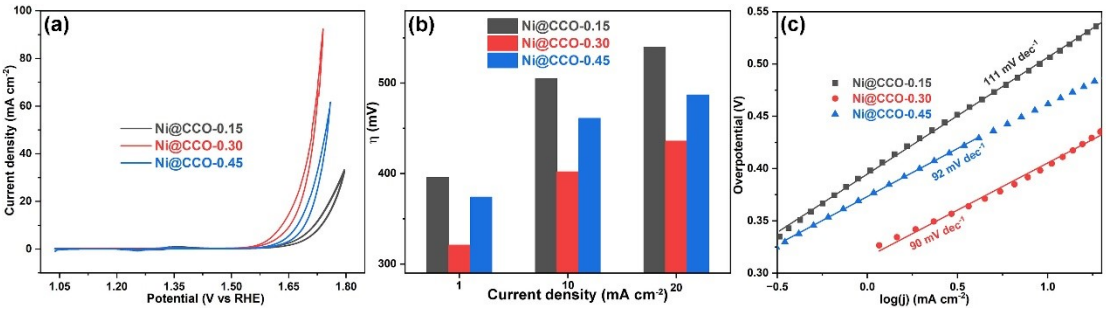

Fig. S11. The CV curves (a), required overpotentials at current densities of 1, 10 and 20 mA cm^{-2} (b) and Tafel slopes (c) of the working electrodes with different $CuCoO_2$ loadings mass (0.15, 0.30 and 0.45 mg cm^{-2}).

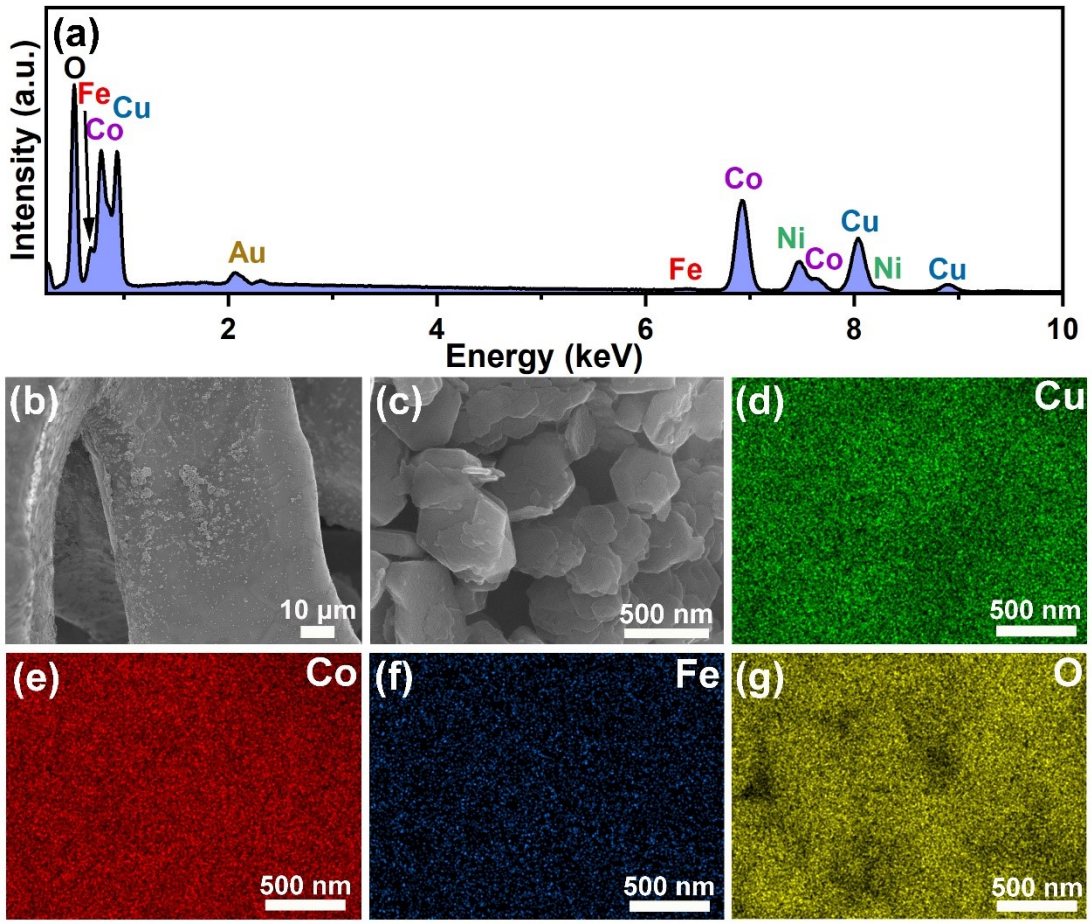

Fig. S12. Elemental analysis report (a), SEM images (b-c) and EDS elemental mappings (c-g) of Ni@3FCCO before OER test.

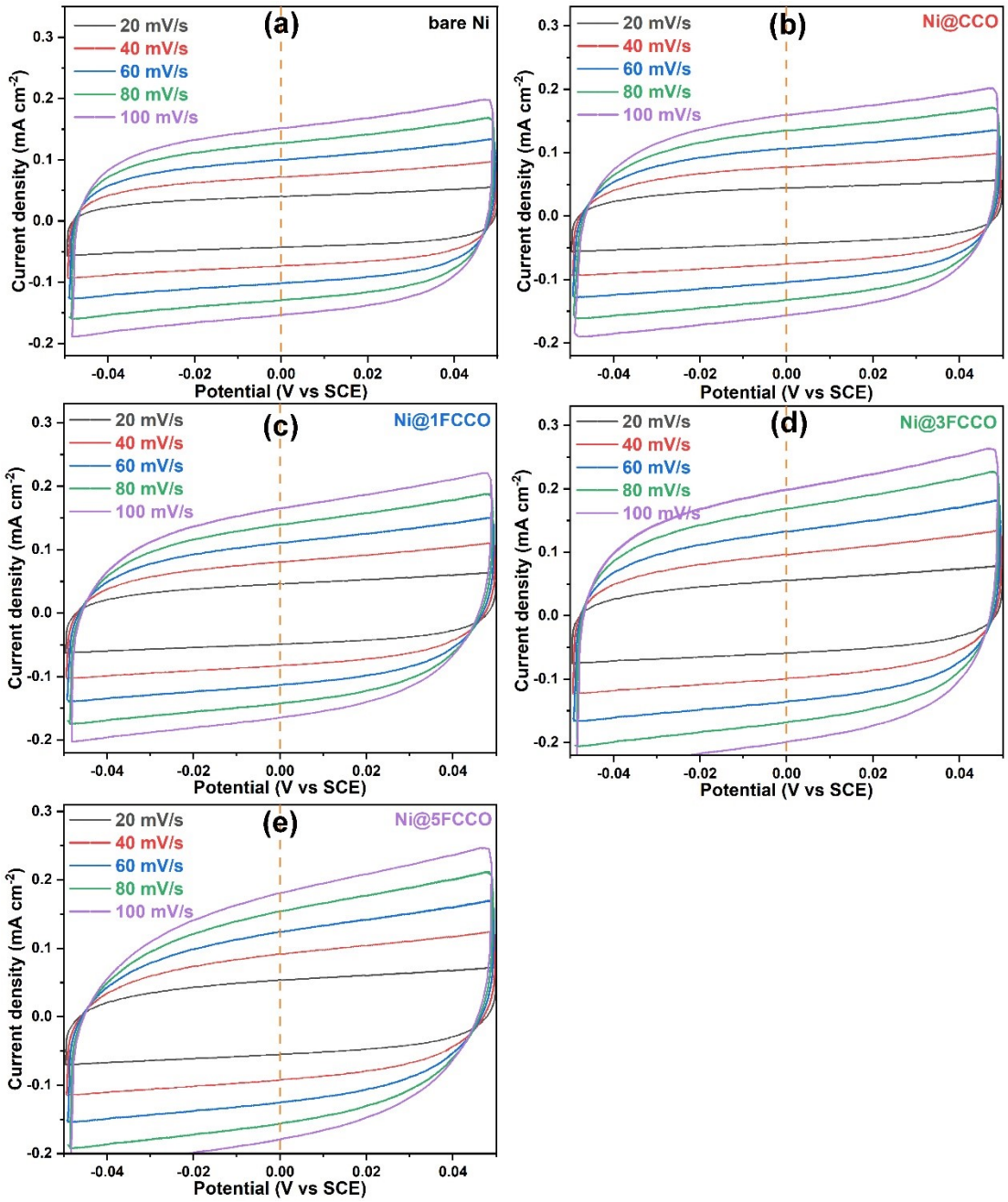

Fig. S13. CV curves at the scan rates from 20 to 100 mV·s^{-1} of bare Ni (a), Ni@CCO (b), Ni@1FCCO (c), Ni@3FCCO (d) and Ni@5FCCO (e) measured in the non-Faradaic region.

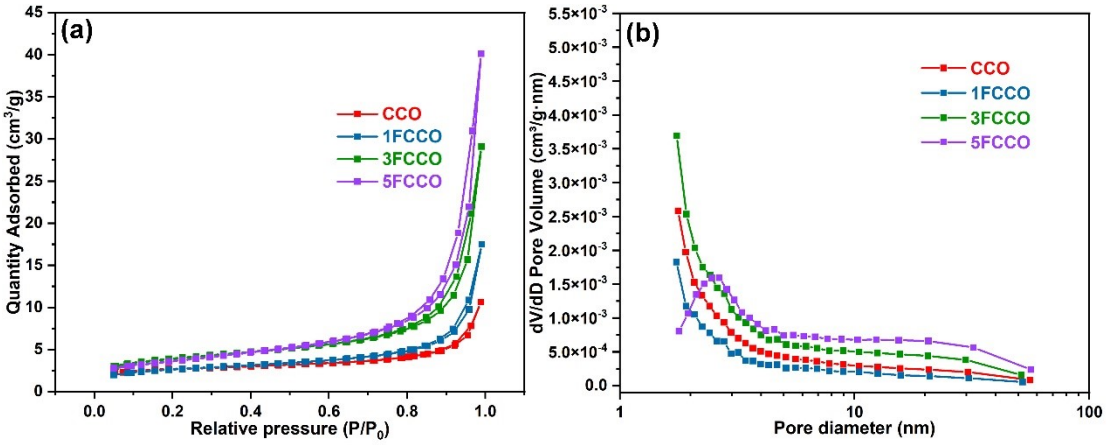

Fig. S14. N_2 adsorption-desorption isotherms (a) and pore structure (b) of CCO, 1FCCO, 3FCCO and 5FCCO powders.

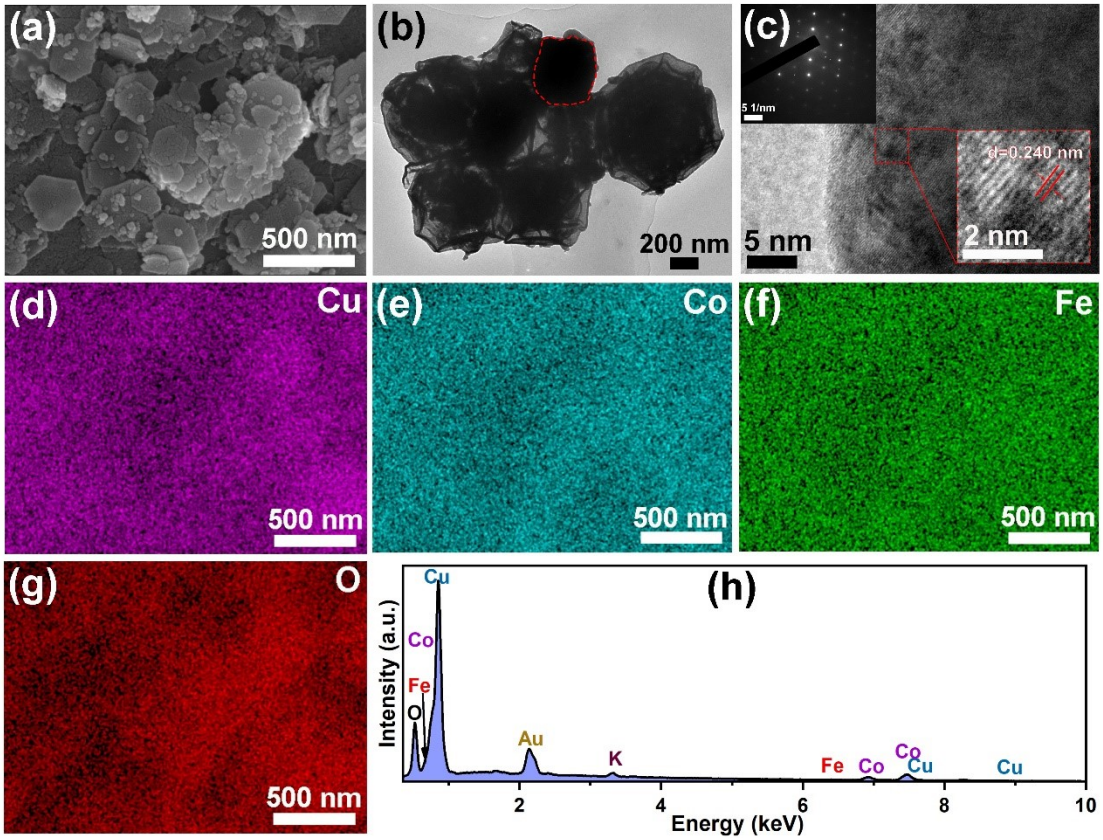

Fig. S15. SEM image (a), TEM image (b), HRTEM image (c), EDS elemental mappings (d-g) and elemental analysis report (h) of Ni@3FCCO after OER. The inset in (c) is SAED.

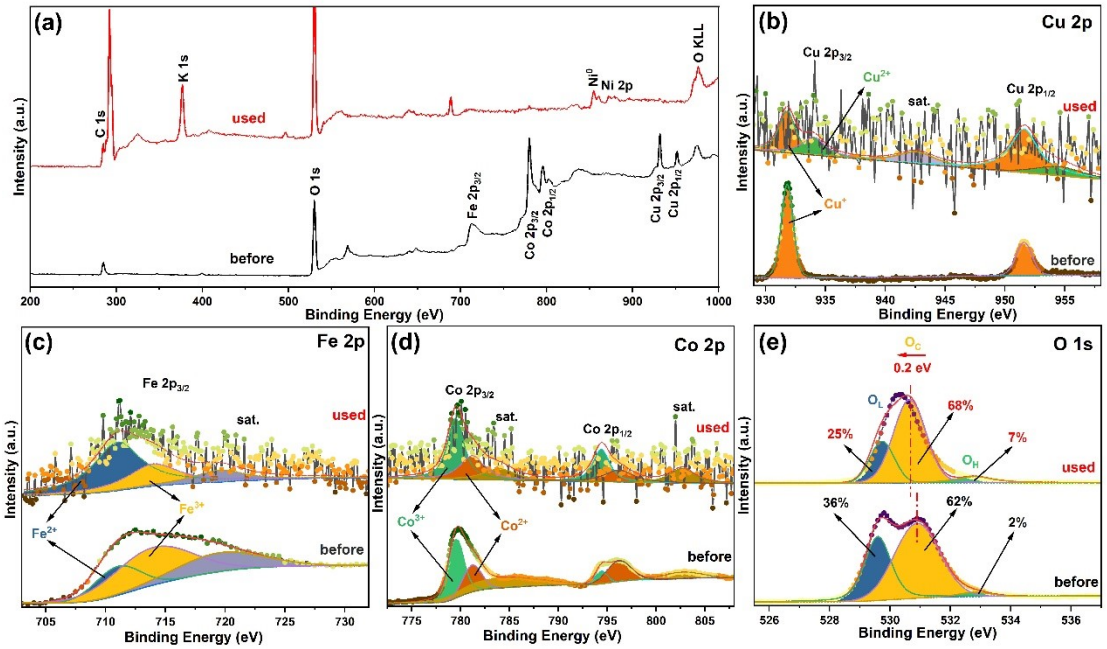

Fig. S16. XPS full spectrums (a) and high-resolution spectrum (b, Cu 2p; c, Fe 2p; d, Co 2p; e, O 1s) of 3FCCO after 18 hours continuous OER stability test.

References:

1. S. Ma, M. Yang, N. Han, L. Shi, L. Wang, J. Bai and D. Xiong, *New Journal of Chemistry*, 2023, **47**, 5216-5223.
2. Z. Du, D. Xiong, S. K. Verma, B. Liu, X. Zhao, L. Liu and H. Li, *Inorganic Chemistry Frontiers*, 2018, **5**, 183-188.
3. D. Xiong, Z. Du, H. Li, J. Xu, J. Li, X. Zhao and L. Liu, *ACS Sustainable Chemistry & Engineering*, 2019, **7**, 1493-1501.
4. Z. Du, J. Qian, J. Bai, H. Li, M. Wang, X. Zhao and D. Xiong, *Inorganic Chemistry*, 2020, **59**, 9889-9899.
5. M. Yang, N. Han, L. Shi, H. Gao, X. Liu, Y. Mi, X. Zeng, J. Bai and D. Xiong, *Dalton Transactions*, 2022, **51**, 8757-8765.
6. Y. Deng, D. Xiong, H. Gao, J. Wu, S. K. Verma, B. Liu and X. Zhao, *Dalton Transactions*, 2020, **49**, 3519-3524.
7. R. Zhang, Z. Sun, C. Zong, Z. Lin, H. Huang, K. Yang, J. Chen, S. Liu, M. Huang, Y. Yang, W. Zhang and Q. Chen, *Nano Energy*, 2019, **57**, 753-760.
8. L. Mao, S. Mohan, S. K. Gupta and Y. Mao, *Materials Chemistry and Physics*, 2022, **278**, 125643.
9. Y. Lu, A. Ma, Y. Yu, R. Tan, C. Liu, P. Zhang, D. Liu and J. Gui, *Journal of Materials Chemistry A*, 2019, **7**, 2906-2910.
10. C. Liu, D. Ji, H. Shi, Z. Wu, H. Huang, Z. Kang and Z. Chen, *Journal of Materials Chemistry A*, 2022, **10**, 1336-1342.
11. Y. Sun, R. Li, X. Chen, J. Wu, Y. Xie, X. Wang, K. Ma, L. Wang, Z. Zhang, Q. Liao, Z. Kang and Y. Zhang, *Advanced Energy Materials*, 2021, **11**, 2003755.
12. S. H. Talib, Z. Lu, X. Yu, K. Ahmad, B. Bashir, Z. Yang and J. Li, *ACS Catalysis*, 2021, **11**, 8929-8941.
13. H. Yuan, S. Wang, X. Gu, B. Tang, J. Li and X. Wang, *Journal of Materials Chemistry A*, 2019, **7**, 19554-19564.
14. R. Elakkiya and G. Maduraiveeran, *Langmuir*, 2020, **36**, 4728-4736.